REGULAR ARTICLE

blood advances

Proteome alterations in erythrocytes with PIEZO1 gain-of-function mutations

Immacolata Andolfo,[1,2,*] Vittoria Monaco,[2,3,*] Flora Cozzolino,[2,3] Barbara Eleni Rosato,[1,2] Roberta Marra,[1,2] Vincenza Cerbone,[2] Valeria Maria Pinto,[4] Gian Luca Forni,[4] Sule Unal,[5] Achille Iolascon,[1,2] Maria Monti,[2,3] and Roberta Russo[1,2]

[1]Dipartimento di Medicina Molecolare e Biotecnologie Mediche, Università degli Studi di Napoli Federico II, Napoli, Italy; [2]CEINGE Biotecnologie Avanzate, Franco Salvatore, Napoli, Italy; [3]Dipartimento di Scienze Chimiche, Università degli Studi di Napoli Federico II, Napoli, Italy; [4]Centro della Microcitemia, delle Anemie Congenite e dei Disordini del Metabolismo del Ferro, EO Ospedali Galliera, Genoa, Italy; and [5]Research Center for Fanconi Anemia and Other Inherited Bone Marrow Failure Syndromes, Department of Pediatric Hematology, Hacettepe University, Ankara, Turkey

Key Points

- Erythrocytes of patients with DHS showed alteration of several processes such as ion transport, proteasome, and vesicle-mediated transport.
- The alteration of the vesicle-mediated transport was functionally demonstrated by an increased vesiculation rate in patients with DHS.

Gain-of-function mutations in PIEZO1 cause dehydrated hereditary stomatocytosis (DHS) or hereditary xerocytosis, an autosomal dominant hemolytic anemia characterized by high reticulocyte count, a tendency to macrocytosis, and mild jaundice, as well as by other variably penetrant clinical features, such as perinatal edema, severe thromboembolic complications after splenectomy, and hepatic iron overload. PIEZO1 mutations in DHS lead to slowed inactivation kinetics of the ion channel and/or facilitation of channel opening in response to physiological stimuli.

To characterize the alterations of red blood cell proteome in patients with mutated PIEZO1, we used a differential approach to compare the proteome of patients with DHS (16 patients from 13 unrelated ancestries) vs healthy individuals. We identified new components in the regulation of the complex landscape of erythrocytes ion and volume balance mediated by PIEZO1. Specifically, the main impaired processes in patients with DHS were ion homeostasis, transmembrane transport, regulation of vesicle-mediated transport, and the proteasomal catabolic process. Functional assays demonstrated coexpression of PIEZO1 and band 3 when PIEZO1 was activated. Moreover, the alteration of the vesicle-mediated transport was functionally demonstrated by an increased vesiculation rate in patients with DHS compared with healthy controls. This finding also provides an explanation of the pathogenetic mechanism underlying the increased thrombotic rate observed in these patients.

Finally, the newly identified proteins, involved in the intracellular signaling pathways altered by PIEZO1 mutations, could be used in the future as potential druggable targets in DHS.

Introduction

PIEZO1 is a mechanosensitive nonspecific cation membrane channel expressed in several tissues in which it plays a crucial role in various physiological processes as a sensor of mechanical forces.[1-8] In

Submitted 1 August 2022; accepted 19 December 2022; prepublished online on *Blood Advances* First Edition 3 January 2023; final version published online 14 June 2023. https://doi.org/10.1182/bloodadvances.2022008673.

*I.A. and V.M. contributed equally to this study.

Data are available on request from the corresponding authors, Immacolata Andolfo (immacolata.andolfo@unina.it) and Maria Monti (montimar@unina.it).

The full-text version of this article contains a data supplement.

red blood cells (RBCs), it is involved in the regulation of hydration and cellular volume. Indeed, gain-of-function (GoF) mutations in PIEZO1 cause dehydrated hereditary stomatocytosis (DHS) or hereditary xerocytosis, autosomal dominant hemolytic anemia characterized by high reticulocyte count, a tendency to macrocytosis, and mild jaundice,[9-13] as well as by other variably penetrant clinical features, such as perinatal edema, severe thromboembolic complications after splenectomy, and hepatic iron overload.[12,14] The phenotype of patients with DHS ranges from asymptomatic to mild anemia.[15,16] The main characteristic of the erythrocyte of DHS is cell dehydration caused by the loss of cellular potassium, which can be assessed by atomic absorption spectroscopy, osmotic fragility, or ektacytometry. PIEZO1 mutations in DHS lead to slowing of inactivation kinetics of the ion channel and/or facilitation of channel opening in response to physiological stimuli.[1,17-19] It is a key sensor of erythrocyte membrane curvature, signaling modulation of intracellular ion content and cell volume as a function of mechanical forces and constraints in capillaries and venules.

PIEZO1 protein exhibits a unique propeller-shaped, 3-bladed homotrimer. Each subunit of the homotrimer contains a peripheral blade containing 38 transmembrane helices, a C-terminal domain, a C-terminal extracellular domain, an anchor, and a 90 Å long beam on the intracellular side. The N-terminal blade is involved in the mechanosensing module, the beam and anchor form the transduction module, and the C-terminal accounts for the ion-conducting pore module.[19-25]

An association of PIEZO1 mechanoreceptor with resistance to erythroid invasion by malarial parasites was observed in vitro and in mice.[26] Indeed, the PIEZO1 E756del reduces the severity of *Plasmodium falciparum* infection in patients with DHS, possibly reflecting decreased RBC surface expression of the plasmodial virulence factor, PfEMP.[27,28] Recent evidence highlighted the role of PIEZO1 in the regulation of iron metabolism in humans and mice. Patients with DHS can exhibit hyperferritinemia (and even hemosiderosis) accompanied by very low values of plasma hepcidin.[29,30]

PIEZO1 influences erythropoiesis because its activation during erythroid differentiation slows differentiation and reticulocyte maturation.[31] To characterize the alterations of RBC proteome in patients with mutated PIEZO1, we used a differential approach to compare the proteomes of patients with DHS with those of healthy individuals. The data improved our knowledge through the identification of new actors in the regulation of the complex PIEZO1-mediated landscape of RBC ion and volume balance. These newly identified players in intracellular signaling pathways aid further understanding of the pathogenetic mechanism of DHS and are potential future druggable targets.

Material and methods

Participant recruitment and sample collection

Overall, 16 patients with a clinical and molecular diagnosis of DHS, and 9 age- and gender-matched healthy control participants (HCs) were included in this study. The average age of participants was 24.0 ± 18.8 years for HCs (5 females and 4 males) and 22.1 ± 17.8 years for patients with DHS (7 females and 9 males). DHS diagnosis was based on history, clinical findings, laboratory data, and genetic testing. The local university ethical committee approved the collection of the patient data (DAIMedLab, "Federico II" University of Naples; N252/18). Blood samples were obtained from the patients after they had given signed informed consent, in accordance with the Declaration of Helsinki. Two additional patients with DHS (patient identifying numbers DHS17 and DHS18) were enrolled for the functional analysis (vesiculation assay).

RBC membrane preparation and immunoblotting

The standard Ficoll-Hypaque (1.077-0.001 kg/L; Sigma-Aldrich, Milan, Italy) density gradient centrifugation method was used to isolate erythrocytes and reticulocytes. The isolated RBCs were diluted in Tris-buffered saline (TBS) to normalize the number of cells on hematocrit values of HCs and patients. Then, RBC cells were lysed by 3 freeze-thaw cycles in 5mM KH_2PO_4 containing a protease inhibitor cocktail (set III, animal-free Calbiochem; Merck KGaA, Darmstadt, Germany). The membrane fraction was sedimented by lysate centrifugation at 36 000 *g* for 20 minutes at 4°C. Erythrocyte membrane extracts (80 µg protein) were loaded on sodium dodecyl sulfate polyacrylamide gels, transferred onto polyvinylidene difluoride membranes (BioRad, Milan, Italy), and incubated with mouse anti-BAND3 glycoprotein antibody (dilution, 1:5000; GTX11012; GeneTex) and mouse anti-ABCB6 antibody (dilution, 1:1000; 101-10003; Raybiotech, Inc). Mouse anti–β-actin antibody (1:12000; SAB1305554; Sigma Aldrich, Milan, Italy) was used as a control for equal loading. Incubation with horseradish peroxidase–conjugated antirabbit immunoglobulin (1:4000) (GE Healthcare, Amersham, United Kingdom) and horseradish peroxidase–conjugated antimouse mmunoglobulin (1:4000) (GE Healthcare) was performed, and labeled bands were visualized (Supersignal West Pico Chemiluminescent Substrate Kit; Thermo Fisher Scientific, Miami, FL). Densitometric analysis was performed with the BioRad Chemidoc using Quantity One software (BioRad).

Protein sample preparation for proteomics analysis

RBC membranes were pooled and washed in phosphate-buffered saline (PBS). Proteins were extracted by adding 5% sodium dodecyl sulfate (BioRad), followed by sonication with 3 pulses of 3 seconds for a total of 5 cycles. Protein extracts were quantified by bicinchoninic acid assay (Thermo Fisher Scientific). The equivalent of 50 µg of each protein sample was digested by trypsin onto S-Trap filters,[32] per the manufacturer's protocol (ProtiFi, Huntington, NY). Peptide mixtures were dried in a SpeedVac system (Thermo Fisher Scientific) and 5 µg of each sample was thereafter subjected to a clean-up by using the zip-tip C18 protocol (Merck, Milan, Italy).

LC-MS/MS analyses and protein identification and quantification

Equal amounts of membrane protein extracts were hydrolyzed with trypsin on S-Trap cartridge and the obtained peptide mixtures were analyzed on a LTQ Orbitrap XL (Thermo Fisher Scientific) coupled to the nanoLC system nanoEasy II. Samples were fractionated onto a C18 capillary reverse-phase column (200 mm, 75 µm, 5 µm) working at a flow rate of 250 nL/min, using a linear gradient of eluent B (0.2% formic acid in 95% acetonitrile) in eluent A (0.2% formic acid in 2% acetonitrile in liquid chromatography mass spectrometry [LC-MS] grade [Merck]) from 5% B to 50% B in 195 minutes. Tandem mass spectrometric (MS/MS) analyses were

performed using the data-dependent acquisition mode: 1 MS scan (mass range from 400 to 1800 mass-to-charge ratio [m/z]) was followed by MS/MS scans of the 10 most abundant ions in each MS scan, applying a dynamic exclusion window of 40 seconds. All samples were run in technical duplicates. For more detail refer to the supplemental Methods.

Multiple-reaction monitoring analyses

Multiple-reaction monitoring (MRM) analysis was carried out for the validation of some proteins found to be differentially expressed in the untargeted proteomic analyses. Specifically, 50 µg of cell lysates obtained from different samples were digested by trypsin onto S-Trap filters, as described earlier. For further details refer to the supplemental Methods.

Functional enrichment analyses

Differentially expressed proteins identified in all sets of analyzed samples were collected in a unique list, which was analyzed using the ClueGO app of Cytoscape. A nonredundant biological processes database of Gene Ontology (GO) was employed by applying the Benjamini-Hochberg correction with a P value $< .05$. For domain-specific functional enrichment analysis, we used PANTHER software to identify slim biological processes of the GO database. Terms with false discovery rates of ≤ 0.05 and an enrichment factor of >5 were selected for the bubble plot representation by the Prism software (GraphPad Software, San Diego, CA).

Immunofluorescence

Peripheral blood from HCs was treated with vehicle (dimethyl sulfoxide), 2.5 µm Yoda1 (10 minutes), or 2.5 µm Yoda1 (20 minutes). Thereafter, RBCs were fixed for 5 minutes in methanol and washed in 50 mM PBS/NH_4Cl. After washing in 1.5 mg/mL EDTA/PBS, blocking was performed with 1% bovine serum albumin/PBS. RBCs were immunologically stained with rabbit anti-PIEZO1 antibody (1:100) (15939-1-AP; Proteintech); mouse anti-BAND3 (BIII-136) antibody (dilution, 1.100 GTX11012; GeneTex), and secondary antibodies (1:100) (Alexa Fluor 488 antirabbit, and Alexa Fluor 568 antimouse, Life Technologies). Coverslips were mounted on microscope slides with 5 uL of moviol. Cells were imaged using a ZEISS LSM980 confocal microscope with Airyscan 2 super-resolution, equipped with an oil immersion plan 63× objective. The following settings were used: green-channel excitation of Alexa488 by the argon laser 488 nm line was detected with the 505 to 550 nm emission bandpass filter. Red-channel excitation of Alexa546 by the helium/neon laser 543 nm line was detected with the 560 to 700 nm emission bandpass filter (using the Meta monochromator). For the quantification of colocalization, 12 independent images for each condition were acquired, with a mean of 7 erythrocytes (standard deviation = ± 3.8) for each acquisition. The intensity values of green (PIEZO1) and red (band 3) channels were extracted to calculate Pearson correlation coefficient of merged regions by Zeiss-ZEN colocalization software.

Extracellular vesiculation assay

Extracellular vesiculation was induced by calcium and ionophore treatment as previously described,[33] with minor modifications. Briefly, RBCs from both HCs and patients with DHS were pelleted and then resuspended in 9 volumes of TBS. $CaCl_2$ (Sigma) at a final concentration of 1 mM and ionophore A23187 (5 µM) (Sigma Aldrich) were used. In addition, samples from both HC and patients with DHS were treated with 5 µM of Yoda1 and then incubated at 37°C for 30 minutes under constant agitation. Treated RBCs were pelleted at 16 000 g for 20 minutes, after which the supernatant was centrifuged for 30 minutes at 16 000 g. The final vesicle pellet was resuspended in an appropriate volume of TBS. Finally, the samples were stained with CD47 (Thermo Fisher Scientific) and glycophorin (Thermo Fisher Scientific) and analyzed by fluorescence-activated cell sorting.[34]

Statistical analysis

Statistical significance of the difference in protein expression was determined using Student t tests. Statistical significance of multiple comparisons was calculated using analysis of variance (ANOVA), and the post hoc correction was performed using Tukey multiple comparison tests. A 2-sided P value $< .05$ was considered statistically significant.

Statistical analysis for the relative protein quantification based on the calculation of label-free quantitation intensities was carried out by MeV software using an unpaired t test with a P value $< .05$. Fold changes (FCs) of statistically significant proteins were calculated for each group of DHS samples as $\log_2$ of the ratio of averaged label-free quantitation intensities of patients vs HCs. Specifically, all proteins with $\log_2 FC < 0.5$ (−0.5) were considered to be downregulated, whereas proteins with $\log_2 FC > 0.5$ (+0.5) were reported as upregulated.

Results

Clinical and genetic findings

We analyzed samples from 16 patients with 13 unrelated ancestries and different PIEZO1 genotypes. Clinical findings of these 16 patients with DHS stratified based on their genotype is summarized in Tables 1 and 2.[14,26,35-38] Specifically, 87.5% of cases exhibited missense variants, whereas 12.5% showed in-frame deletions. Herein, we report unpublished data from 8 patients and 2 additional PIEZO1 variants not yet associated with DHS1 (c.6205G>A, p.Val2069Met; c.4274G>A, p.Ser1425Asn) (Table 1). In agreement with the autosomal inheritance pattern of DHS, 11 patients showed pathogenic variants in heterozygous state whereas 5 were in homozygous state.

As previously described, the mutations were distributed along the entire coding sequence of the gene. Specifically, in most of the cases (75%) the variants localized in the mechanosensing module (a repetitive structural unit called the transmembrane helical unit [THU], or Piezo repeat; ie, THU4, THU5, THU7, THU8), in only 12.5% of cases the mutations localized in the transduction module (Anchor), whereas in the remaining 12.5% of cases, the mutations localized in the ion-conducting pore (cover of the channel [CAP] and a beam, roughly at the bottom of the third Piezo repeat or THU [CLASP]).

Differential proteomic analysis in patients carrying PIEZO1 mutations

Differential proteomic analyses were carried out on erythrocyte membrane proteins from patients with DHS (n = 16) and HCs (n = 9). Differentially expressed proteins were identified, and analyses

Table 1. Genetic features of the patients with PIEZO1 variants analyzed in this study

Patient ID	HGVS (Coding)*	HGVS (protein)	RefSeq ID	HGMD	Zygosity	Protein domain	Protein domain function	Published patient data (Y/N)	Published variant
DHS1	c.6328C>T	p.Arg2110Trp	rs776531529	CM1911800	Het	Anchor	Transduction module	Y	12,35
DHS2	c.1815G > A	p.Met605Ile	-	CM1911750	Het	THU4	Mechanosensing module	Y	12,38
DHS3	c.2268_2270delGGA	p.Glu756del	rs572934641	CD184712	Het	THU5	Mechanosensing module	N	26
DHS4	c.2268_2270delGGA	p.Glu756del	rs572934641	CD184712	Het	THU5	Mechanosensing module	N	26
DHS5	c.4766C>T	p.Thr1589Ile	rs534283978	CM1914354	Het	Close to CLASP	Ion-conducting pore	N	36
DHS6	c.5195C>T	p.Thr1732Met	rs139051768	CM200163	Het	THU8	Mechanosensing module	N	35
DHS7	c.2005G>T	p.Asp669Tyr		CM1817546	Het	THU4	Mechanosensing module	Y	14
DHS8	c.2005G>T	p.Asp669Tyr		CM1817546	Het	THU4	Mechanosensing module	Y	14
DHS9	c.1815G > A	p.Met605Ile	-	CM1911750	Het	THU4	Mechanosensing module	Y	38
DHS10	c.6205G>A	p.Val2069Met	rs199752762	-	Het	Close to Anchor	Transduction module	N	-
DHS11	c.6796G>A	p.Val2266Ile	rs546338962	CM187363	Het	CAP (CED)	Ion-conducting pore	Y	37,38
DHS12	c.4274G>A	p.Ser1425Asn	rs772788410	-	Hom	THU7	Mechanosensing module	N	-
DHS13	c.4274G>A	p.Ser1425Asn	rs772788410	-	Hom	THU7	Mechanosensing module	N	-
DHS14	c.5389C>T	p.Arg1797Cys	-	CM187402	Hom	THU8	Mechanosensing module	Y	37
DHS15	c.5389C>T	p.Arg1797Cys	-	CM187402	Hom	THU8	Mechanosensing module	Y	37
DHS16	c.5389C>T	p.Arg1797Cys	-	CM187402	Hom	THU8	Mechanosensing module	N	37

CED, C-terminal extracellular domain; Het, heterozygous; Hom, homozygous; N, not; Y, yes; HGVS, Human Genome Variation Society.
*The transcript reference of the *PIEZO1* gene is NM_001142864.4

Table 2. Clinical features of the patients with PIEZO1 variants analyzed in this study

	Age	Gender	RBC	Hb	Hct	MCV	MCH	MCHC	ARC	Total bilirubin	LDH	Ferritin
Code	y	M/F	$\times 10^6/\mu L$	g/dL	%	fL	pg	g/dL	$\times 10^3/\mu L$	mg/dL	U/L	µg/L
DHS1	50	M	4.4	14.9	44.2	100.0	33.7	33.7	380.0	5.7	335.0	1180.0
DHS2	35	M	4.6	16.0	43.7	94.4	34.6	36.6	130.0	2.8	210.0	293.0
DHS3	49	M	5.7	16.8	47.1	82.6	29.4	35.6	113.0	1.1	251.0	294.0
DHS4	18	F	5.1	13.4	40.0	92.0	29.1	31.6	69.0	1.5	530.0	126.0
DHS5	36	M	2.7	8.6	26.8	99.9	32.2	32.2	905.0	7.3	192.0	32.0
DHS6	53	M	5.0	15.1	46.0	93.1	30.3	32.5	442.0	2.3	8.9	789.0
DHS7	30	F	3.4	13.5	37.7	111.0	40.0	38.2	-	-	1.4	775.0
DHS8	20	F	3.6	11.9	33.2	92.2	33.1	36.0	-	-	235.0	312.0
DHS9	13	F	4.0	13.0	0.0	88.4	-	36.7	217.0	13.0	-	-
DHS10	15	F	6.1	10.8	33.9	55.2	17.6	31.9	896.0	1.3	210.0	31.5
DHS11	14	F	2.8	10.9	31.4	110.0	38.2	34.6	535.0	1.9	253.0	355.0
DHS12	1	M	3.0	8.8	26.7	89.7	29.6	33.0	127.0	0.6	307.0	556.0
DHS13	6	F	3.8	11.0	34.6	91.9	29.2	31.8	189.0	0.4	328.0	48.3
DHS14	3	M	3.6	11.7	33.8	94.0	31.5	33.5	165.0	4.6	315.0	488.0
DHS15	4	M	3.8	11.7	34.8	90.7	30.5	33.7	145.0	4.3	250.0	72.0
DHS16	6	M	4.2	12.8	37.8	90.7	30.6	33.8	266.0	1.4	316.0	68.0

ARC, absolute reticulocyte count; F, female; Hb, hemoglobin; Ht, hematocrit; LDH, lactate dehydrogenase; M, male; MCH, mean corpuscular hemoglobin; MCHC, mean corpuscular hemoglobin concentration; MCV, mean corpuscular volume.

produced a unique list of 171 total proteins (supplemental Table 2). The identified proteins were subdivided based on the localization of the mutations in the different domains of PIEZO1 (Figure 1A). Among the 171 differentially expressed proteins, 142 were upregulated, and 29 were downregulated. A total of 139 proteins were altered in a specific domain, whereas 40 proteins were shared between different domains (Figure 1A).

The largest number of differentially expressed proteins belonged to the THU7 and THU8 domains. Functional enrichment analysis highlighted that most of the upregulated proteins were linked to a few molecular processes, independent of the position of mutations (Figure 1B). The most enriched molecular processes were exocytosis, vesicle-mediated transport to the plasma membrane, vesicle budding from the membrane, P-type adenosine triphosphatase (ATPase)-coupled transmembrane transporter activity, and regulation of oxidative stress. Exocytosis is the last step of the secretory pathway that involves the fusion of vesicles with the plasma membrane. RBCs experience membrane loss by exocytosis, both in vivo and during storage, by the blebbing of microvesicles from the tips of echinocytic spicules.[39]

Rab5c was 1 of the most upregulated proteins in patients with DHS compared with HCs. Members of the Rab protein family are small guanosine triphosphatases of the Ras superfamily that are thought to ensure fidelity in the process of docking and/or fusion of vesicles with their correct acceptor compartment. Rab5c-mediated endocytic trafficking is also essential in hematopoietic stem and progenitor cell development.

The most upregulated proteins within the regulation of oxidative stress process were basigin (BSG), protein disulfide-isomerase (P4HB, also called PDI), peptidyl-prolyl cis-trans isomerase A, and thioredoxin (TXN). P4HB/PDI regulates the formation and rearrangement of disulfide bonds. This protein is present in the human erythrocyte membrane. In sickle cell disease, cell surface–associated PDI shows increased activity that is related to the regulation of erythrocytes oxidative stress and hydration status.[40] TXN is 1 of the main antioxidants with a scavenger function of reactive oxygen species, and its levels are increased in oxidation damage during inflammation disease.[41] Peptidyl-prolyl cis-trans isomerase A induces the chemotaxis and signaling by its peptidyl-prolyl isomerase activity or by binding basigin protein, thus regulating reactive oxygen species production and, therefore, the oxidative stress and the inflammatory response.[42]

The functional process named ATPase-coupled transmembrane transporter activity includes a large number of proteins involved in the transport of ions; ATPase plasma membrane Ca^{2+} transporting 1 (ATP2B1, PMCA1); ATPase plasma membrane Ca^{2+} transporting 4 (ATP2B4, PMCA4); ATPase Na^+/K^+ transporting subunit alpha 1 (ATP1A1); aquaporin-1 (AQP1), a water-specific channel; solute farrier Family 40 member 1 (SLC40A1) or ferroportin (FPN), that is, the only known vertebrate iron exporter; and ATP-binding cassette subfamily B member 6, mitochondrial (ABCB6), whose mutations are causative of another hereditary RBC membrane transport defects, the familial pseudohyperkalemia. In addition, we observed upregulation of the solute carrier family 4 member 1 (SLC4A1, band3), the major mediator of the exchange of chloride with bicarbonate across plasma membranes; lysine deficient protein kinase 1 (WNK1); and odd-skipped related transcription factor 1 (OSR1); all of which are known to be involved in cation homeostasis and trafficking regulation.

Intriguingly, among all significant biological processes, we found a single downregulated cluster into which almost all the downregulated proteins converged; this regulation of hematopoietic

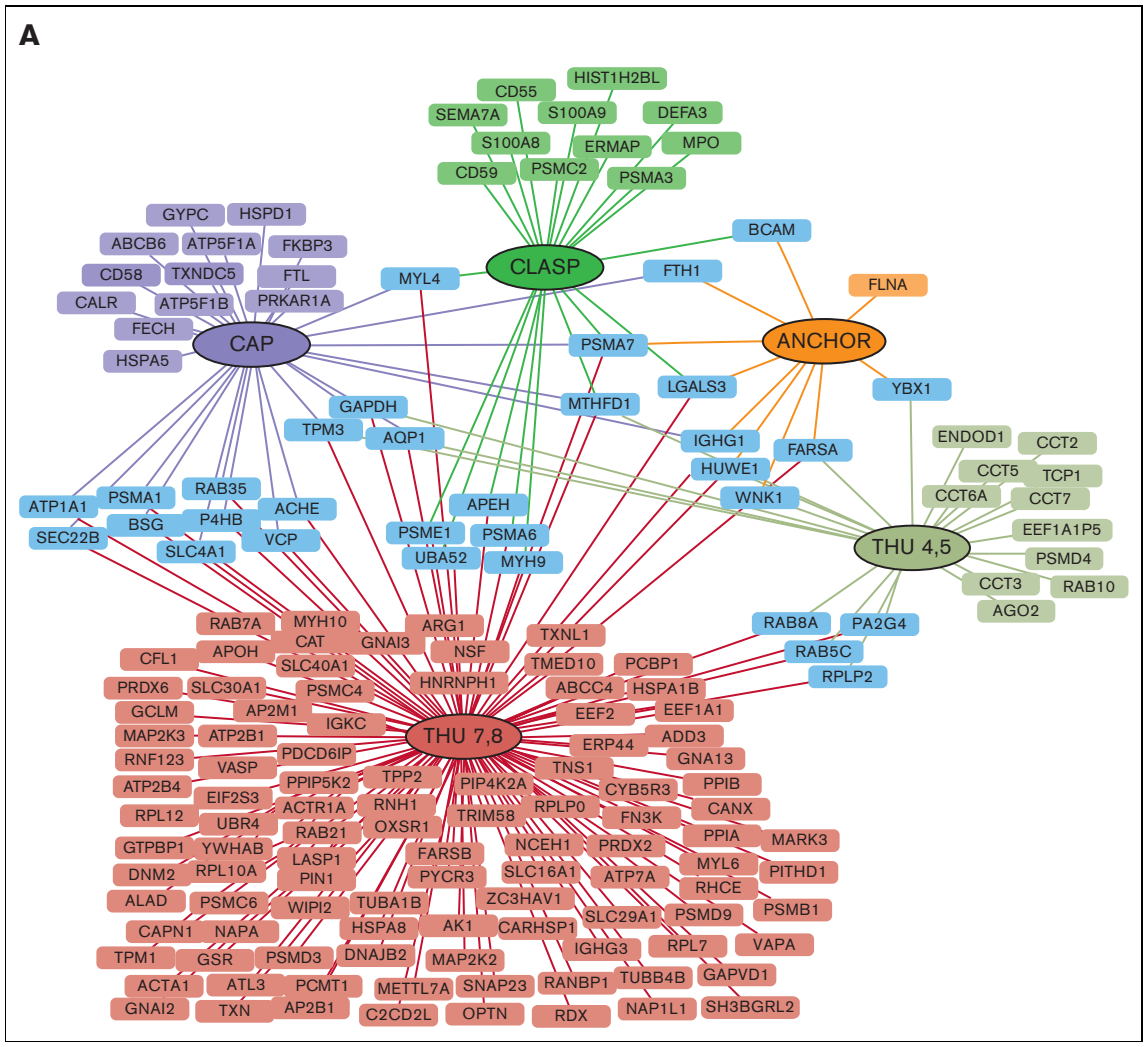

Figure 1. Differentially expressed proteins (clustered for PIEZO1 protein domains) in patients with DHS compared with HCs. (A) Cytoscape graphical representation of proteins identified as differentially expressed in proteomic analyses, and clustered based on their identification within patient samples carrying a mutation in specific domains of PIEZO1. Red boxes refer to proteins identified in patients heterozygous and homozygous for mutations in THU7-THU8 domains; half red and yellow boxes indicate proteins solely shared between patients heterozygous and homozygous for mutation in THU7-THU8 domains. Purple, dark green, orange, and light green boxes refer to proteins specifically identified in patients that are heterozygous carrying mutations in CAP, CLASP, ANCHOR, and THU4-5 domains, respectively. Light-blue boxes refer to proteins differentially expressed and shared between at least 2 different conditions. (B) ClueGO functional analysis representation of biological processes including all differentially expressed proteins. GO was used as database; a *P* value Benjamini-Hochberg correction cutoff of 0.05 was applied. Cluster 1 in pink and cluster 2 in blue represent upregulated and downregulated, respectively. Node sizes were correlated with the specific *P* value.

stem cell differentiation functional group includes almost only proteasome 20S subunits (PSMA1, PSMA3, PSMA6, PSMA7, and PSMB1) that were all downregulated in patients with DHS compared with HCs.

We further subdivided our case series into 2 main groups based on the different mutated domains, the mechanosensing module (domains THU4, THU5, THU7, THU8, and CLASP), and the transduction module/ion-conducting pore, which included only 2 patients. The functional enrichment analysis allowed the association of specific functional processes with each domain. The ion homeostasis/transmembrane transport processes were prevalently impaired in patients carrying mutations in the transduction module/ion-conducting pore domain; conversely, the mechanosensing module was found mainly associated with regulation of the vesicle-mediated transport process. The only process common to both groups was the proteasomal protein catabolism process, as was expected from the recurrent identification of downregulated proteasomal subunits in a large portion of patient samples (supplemental Figure 1).

PIEZO1 GoF mutations cause increased phosphorylation of OSR1

Four different proteins (WINK1 and OSR1, both related to the dysregulation of the cation transport pathway; RAB35 and RAB8A, related to the vesicle/endocytosis process) were validated by using an innovative method based on MS/MS MRM. Briefly, for each

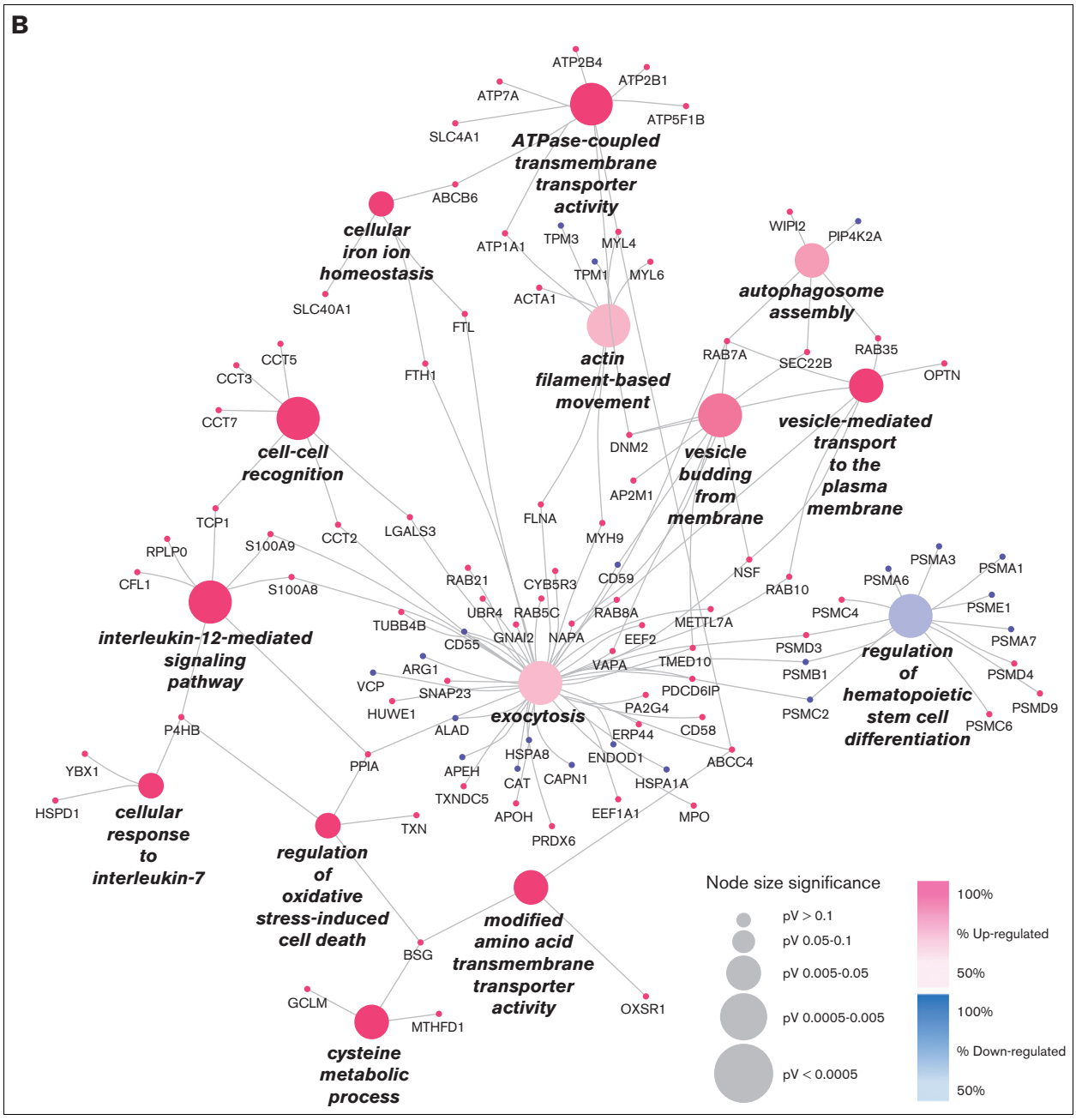

Figure 1 (continued)

protein, at least 3 prototypic peptides were selected and at least 3 transitions per protein were monitored. Total transition areas normalized to endogenous actin signals were used for the statistical analysis and fold-change calculations. Based on differential proteomics data, RAB35, RAB8A, and WINK1 were upregulated in the patients with DHS when compared with HCs; whereas OSR1 was overexpressed only in patients carrying mutations in the mechanosensing module of PIEZO1 (Figure 2A-B). Moreover, further investigation of OSR1 and WNK1 was carried out for 3 reasons: (1) band 3 interacts directly with WNK1, (2) deoxyhemoglobin-induced displacement of WNK1 from band 3 initiates a signaling cascade resulting in phosphorylation/activation of OSR1 and phosphorylation/activation of NKCC1, and (3) mutations leading to either elimination or augmentation of the deoxyhemoglobin binding site on band 3 cause dissociation of WNK1 from band 3.[43] Therefore, we assayed the level of phosphorylation of OSR1 on threonine 185 (ie, the site of phosphorylation by WNK1 kinase).[44] in patients with DHS carrying PIEZO1 variants in the mechanosensing module. MRM relative quantification data on tryptic peptide (185 to 202), which contains threonine185 showed that, besides the expected accumulation of nonphosphorylated peptide in patients with DHS compared with HCs, the phosphorylated form is more abundant in patients carrying PIEZO1 variants in the mechanosensing module (Figure 2B).

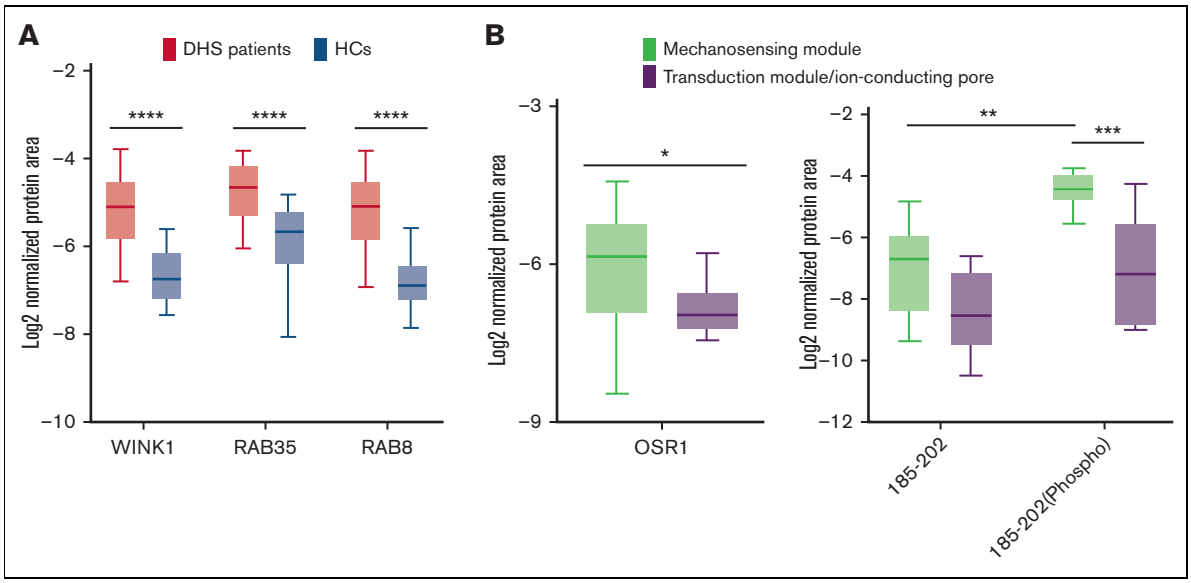

Figure 2. Validation analysis of the transport, vesicle, and endocytosis pathways by multiple-reaction monitoring analysis. (A) Graphic representation obtained by the GraphPad software of the log2 normalized mean areas for all the proteins validated in patients with DHS (red boxes) compared with HCs (blue boxes). (B) Left: expression levels of OSR1 protein in patients with DHS with mutations in the mechanosensing module (green boxes) compared with patients with transduction module/ion-conducting pore mutations (purple boxes). Right: phosphorylation state analysis of OSR1 peptide (from amino acid 185-202) phosphorylated and nonphosphorylated in patients with DHS with mutations in the mechanosensing module (green boxes) compared with patients with transduction module/ion-conducting pore mutations (purple boxes). The representations were obtained by GraphPad software. A 2-way ANOVA test in a multiple comparison way was applied; *$P \leq .05$; **$P \leq .01$; ***$P \leq .001$; and ****$P \leq .0001$.

PIEZO1 GoF mutations induce an augmented production of extracellular vesicles

The vesicle pathway involvement was further analyzed by studying the extracellular vesicle (EV) content in blood samples from 2 HCs treated with PIEZO1 activator, Yoda1, to mimic the function of PIEZO1 mutations and in 2 patients (DHS17 carrying the variant p.Gly1394del and DHS18 carrying the variant p.Lys2502Arg). Using fluorescence-activated cell sorting analysis, we analyzed the percentage of cells that were double positive for the CD47 and CD235a markers, representing the population of EVs. We found that, at steady state, the 2 patients presented an increased percentage of cells double positive for CD47 and CD235a markers and, therefore, an increased level of EVs (Figure 3A-B). After the treatment with $CaCl_2$ and Yoda1, HCs showed an increased level of EVs compared with nontreated samples. Patient DHS17 presented an increased percentage of EVs compared with HCs, even after tretament with CaCl2 and Yoda1; in contrast, patient DHS18 only showed a trend of increased EVs levels, although not statistically significant (Figure 3A-B).

PIEZO1 GoF mutations cause colocalization of PIEZO1 with band 3

To validate the deregulation of transmembrane transporter activity, we focused our attention on band 3, the most representative protein of the plasma membrane of RBCs, and ABCB6, strictly related to PIEZO1 by causing another RBC membrane defect. Western blotting analysis confirmed the upregulation of both band 3 and ABCB6 proteins in the patients with DHS compared with HCs (Figure 4A). We hypothesized that the upregulation of band 3 in patients with DHS could be related to enhanced interaction between PIEZO1 and band 3. Thus, we analyzed the protein localization of band 3 and PIEZO1 by super-resolution confocal microscopy in the erythrocytes of HCs at the steady state and during a time course (10 and 20 minutes) of treatment with Yoda1 (chemical activator of PIEZO1) to mimic the hyperactivation of the channel present in the patients with GoF variants in PIEZO1. We observed a significant positive correlation between an increased time of exposure to Yoda1 and improved colocalization of band 3 and PIEZO1 at the plasma membrane of RBCs (Figure 4B-C).

Discussion

PIEZO1 protein reportedly functions as a pore-forming mechanosensitive ion channel in a wide range of animals.[45] It is distributed mainly in nonsensory tissues, regulating osmotic homeostasis, proprioception, and light touch in humans.[46]

PIEZO1 has been linked to different human diseases, such as DHS caused by GoF mutations and congenital lymphatic dysplasia owing to loss-of-function mutations.[16] Currently, most of the DHS causative variants have not yet been characterized. To understand the pathogenic mechanisms underlying PIEZO1 GoF variants, we analyzed the plasma membrane proteome of RBCs isolated from patients with DHS compared with that in HCs. We enrolled 16 patients with DHS with mutations localized in different domains of the PIEZO1 protein, spanning THU (mechanosensing module), the transduction module (Anchor), and the ion-conducting pore (CAP and CLASP). We found 171 differentially expressed proteins (142 were upregulated and 29 downregulated) between patients and HCs. The most impaired biological processes were

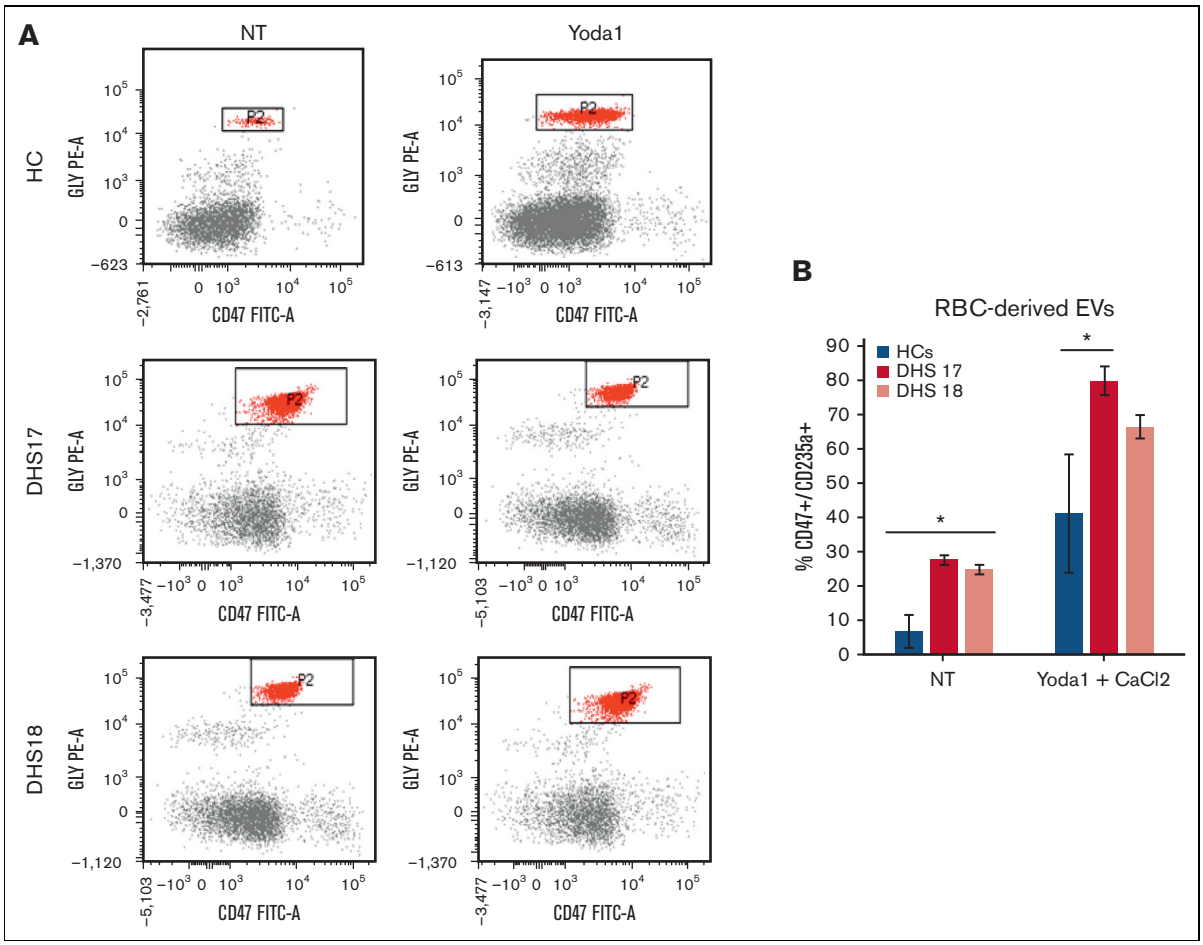

Figure 3. Increased levels of RBC-derived EVs in patients with PIEZO1 GoF mutations. (A) Flow cytometry analysis for RBC-derived EVs. Glycophorin A or CD235a, y-axis, and CD47 (x-axis) (axis values in log scale). Window P2 has $CD235a^{+}/Cd47^{+}$ cell populations that represent RBC-derived EVs. The analysis was performed in blood samples from HCs and 2 patients with DHS with PIEZO1 mutations (DHS17 and DHS18), not treated or treated with Yoda1 (PIEZO1 activator) and $CaCl_2$. (B) RBC-derived EVs numbers in samples from flow cytometry analysis shown in panel A.

ATPase-coupled transmembrane transporter activity, exocytosis, vesicle-mediated transport to the plasma membrane, and vesicle budding from the membrane, which are all connected to alterations of intracellular protein trafficking. The proteins belonging to these processes are transmembrane channels involved in the transport of ions across the membrane, such as ATP2B1, ATP2B4, ATP1A1, RHCE, ATP7A, SLC16A1, SLC29A1, and AQP1. These findings demonstrated that PIEZO1 GoF mutations contribute to altered ionic homeostasis by directly or indirectly affecting the expression of other ion channels. The increased expression of AQP1 correlates with the dehydration of the RBCs observed in DHS.

Of note, FPN was upregulated in patients with DHS compared with controls. FPN is highly abundant in erythrocytes and protects them against oxidative stress and malaria infection.[47] FPN occurs at 54 000 copies per cell, an amount greater than that of the integral RBC membrane protein component, glycophorin C. FPN is critical for exporting free iron generated by hemoglobin autoxidation to maintain the integrity of mature RBCs. Interestingly, FPN activity is inhibited by hepcidin, the key regulator hormone of iron homeostasis, also in mature RBCs. Therefore, the increased level of FPN could be related to the lower levels of plasma hepcidin encountered in patients with DHS.[29] Moreover, in RBCs of patients with DHS there are elevated levels of calcium,[1] an important FPN cofactor stimulating iron efflux by carrying out a regulatory function in FPN-mediated iron efflux.[48] The combined and additive effects of both hepcidin and dysregulated calcium levels in patients with DHS could strictly be related to the altered expression level of FPN.

In addition, ABCB6 was overexpressed in DHS compared with controls. ABCB6 is an erythrocyte membrane ABC transporter protein bearing the Langereis blood group antigen system in RBCs and porphyrin transporter. GoF mutations in ABCB6 cause isolated familial pseudohyperkalemia (included in the large class of hereditary stomatocytosis), a dominant RBC trait characterized by cold-induced "passive leakage" of RBC potassium ions into plasma. Overexpression of this protein in RBCs could enhance potassium efflux and induce hyperkalemia as recurrently found in patients with DHS with pleiotropic syndrome.[10]

The erythrocyte anion exchanger (AE1, SLC4A1, band 3), the most abundant protein in the RBCs membrane with 10^6 copies per erythrocyte, also showed increased expression in DHS compared

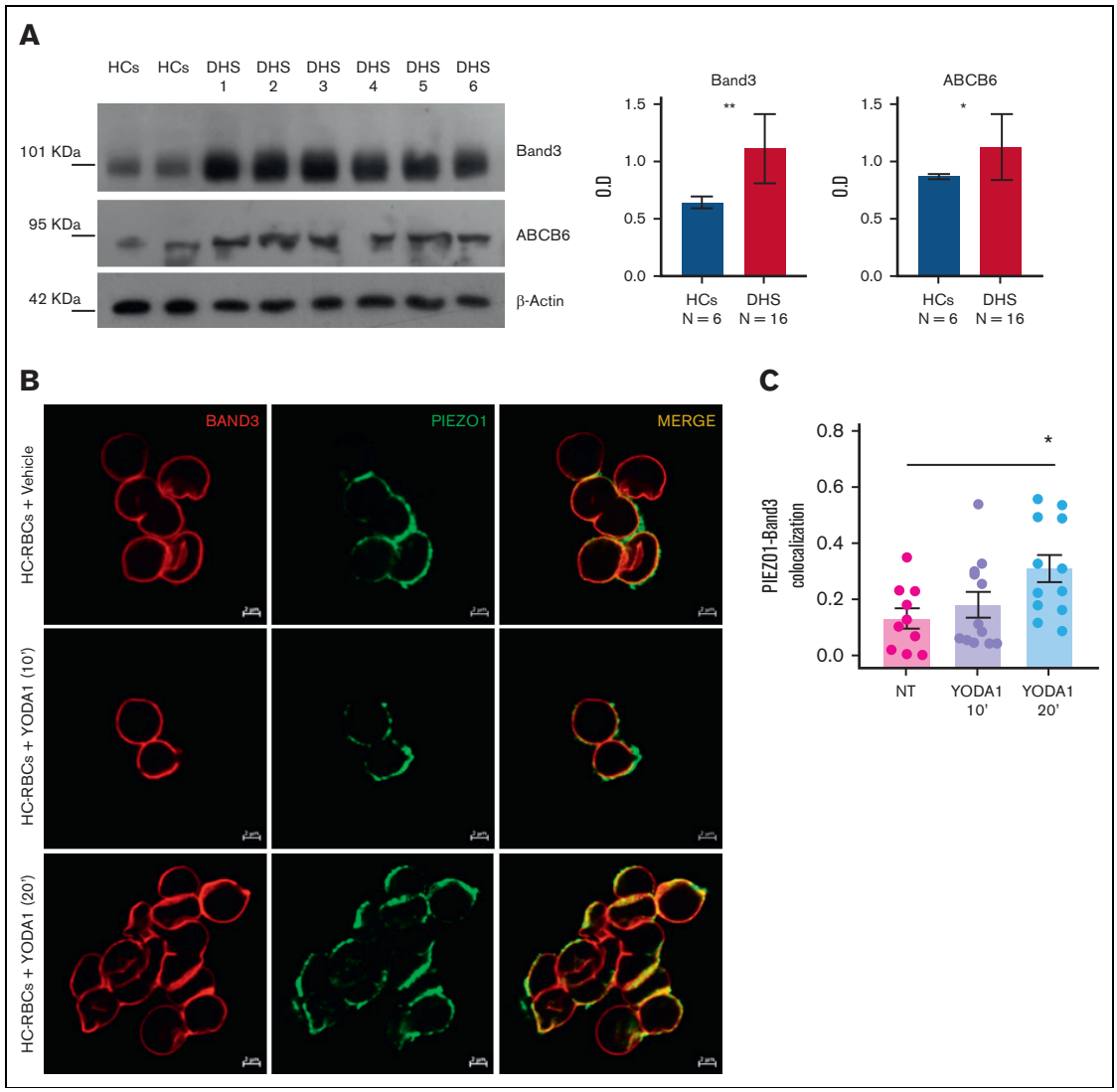

Figure 4. Band 3 and ABCB6 overexpression in plasma membrane protein of RBCs from patients with DHS and PIEZO1–band 3 colocalization. (A) Left: representative immunoblot of RBC membrane proteins showing band 3 and ABCB6 protein expression normalized to β-actin in the patients DHS1, DHS2, DHS3, DHS4, DHS5, and DHS6 compared with HCs (2 pools of HCs, each of n = 3). Right: densitometric analysis of 3 representative western blotting is shown for band 3 and ABCB6 proteins. Data are presented as mean ± standard deviation; $*P < .05$; $**P < .01$ (Student *t* test). (B) Representative confocal imaging by ZEISS LSM 980 Airyscan 2 of HC RBCs treated with vehicle (upper panel) compared with HC RBCs treated with 2.5 μM Yoda1 (10 minutes) (middle panel) and HC RBCs treated with 2.5 μM Yoda1 (20 minutes) (lower panel). Rabbit anti-PIEZO1 antibody is shown in green, mouse anti–band 3 is shown in red. The overlapping of both signals (MERGE) is shown on the right (yellow). (C) Quantification by Pearson correlation of PIEZO1–band 3 colocalization in untreated HC RBCs, HC RBCs + 2.5 μM Yoda1 (10 minutes), and HC RBCs + 2.5 μM Yoda1 (20 minutes) is shown. Data shown are the means of 12 independent acquisitions ± standard error of the mean; $P < .05$ for trend (ANOVA test), $*P < .05$ (post hoc correction by Tukey multiple comparisons test).

with HCs. Specific mutations in the *SLC4A1* gene result in several erythrocyte diseases, that is, hereditary spherocytosis or hereditary stomatocytosis and/or kidney disease dominant distal renal tubular acidosis.[15] The overexpression of band 3 could potentiate the ion unbalance in RBCs of patients with DHS. Besides a functional interaction between band 3 and PIEZO1, we hypothesize a possible physical interaction. Therefore, a colocalization analysis by super-resolution confocal microscopy of RBCs from HCs treated with the PIEZO1 activator Yoda1 to mimic the alterations of PIEZO1 found in patients with DHS was performed. Interestingly, an increased colocalization of PIEZO1–band 3 was detected when the RBCs were treated with Yoda1. This finding suggests a possible interaction of these 2 proteins when PIEZO1 is opened and activated. Thus, band 3 could participate in the complex pathological mechanism of ion balance alteration in DHS through both a direct and indirect action on ion homeostasis. Moreover, it is interesting to note that PIEZO1 can both curve the lipid membranes and respond directly to the changes in membrane tension associated with changes in membrane curvature.[49] The curvature of the membrane induced by PIEZO1[50] likely requires strong protein-lipid interactions to anchor the bilayer around the curved shape of PIEZO1. In addition, the function of band 3 may be

influenced by the interactions between band 3 and lipids or lipid domains in the plasma membrane.[51] Indeed, the curvature of the membrane induced by PIEZO1 seems to get closer to band 3 and could regulate its activity.

Furthermore, we found upregulation of WNK1 and OSR1, both involved in cation homeostasis and trafficking regulation in RBCs. Deoxyhemoglobin (but not oxyhemoglobin) binds to the cytoplasmic domain of band 3 and displaces WNK1 kinase from its docking site on band 3. The displacement of WNK1 kinase activates OSR1 by phosphorylating threonine 185, which in turn phosphorylates and activates NKCC1, leading to an influx of NaCl and KCl into the cell whenever O_2 levels decrease. In this manner, the O_2 content of the erythrocyte can modulate erythrocyte volume during RBC transit in the vasculature.[43] The increased levels of WNK1, OSR1, and phosphorylated OSR1 may have a synergic effect on the dysregulation of NaCl and KCl influx in RBCs of patients with DHS.

In patients with DHS, we identified several upregulated proteins belonging to the vesiculation process. To assess whether the increased level of these proteins could be involved in the alterations of vesicle production, we analyzed the EVs content in HCs and patients with DHS. We demonstrated, to the best of our knowledge, for the first time, an increased level of EVs in both HCs treated with Yoda1 (mimicking the PIEZO1 activation) and patients with DHS compared with nontreated samples. RBC-derived EVs are secreted during erythropoiesis, physiological cellular aging, disease conditions, and in response to environmental stressors. Under physiological and pathological conditions, RBC-derived EVs loaded with proteins, lipids, and microRNAs might be vital for communication with the endothelium to regulate NO and O_2 homeostasis, redox balance, and immunomodulation. Furthermore, RBC-derived EVs are critical to the dysregulation of hemostasis and demonstrate relevant procoagulant effects in several disease states.[52] Moreover, RBC-derived EVs are involved in the complex iron metabolism process because they carry ferritin and express transferrin receptors.[53] The increased level of RBC-derived EVs in patients with DHS could explain the increase in severe thromboembolic events after splenectomy, and studying this aspect could open new avenues in the pharmacological treatment of these complications.

Several proteins involved in the oxidative stress process were upregulated, whereas a single downregulated cluster, called regulation of hematopoietic stem cell differentiation, mainly included proteasome subunits. Proteasomes are multicatalytic complexes with important roles in the protein control of the RBC membrane proteome. The 20S complex is the proteolytic core of the proteasome, equipped with 3 proteolytic activities: caspase like, trypsin like, and chymotrypsin like. Misfolded proteins are transferred in the 20S cylinder after being selected by 19S regulatory complexes that recognize ubiquitinated molecules. There is a time-dependent translocation and/or activation of the proteasome in the membrane of RBC and a tight connection of activity with the oxidative burden of RBCs. In RBCs of DHS, downregulation of proteasomes could account for an impairment of protein control in addition to increased oxidative stress. This finding is very different compared with other anemias such as sickle cell disease and glucose-6-phosphate dehydrogenase deficiency,[54] and raises a question about the possible role of PIEZO1 as a regulator of the proteasome.

To the best of our knowledge, this study identified for the first time alterations within the RBC proteome of patients affected by DHS. It showed new pathophysiological mechanisms in DHS and identified potentially targetable proteins in this condition characterized by the absence of therapeutical options.

Acknowledgments

The authors thank the facility of flow cytometry. The local University Ethical Committee approved the collection of the patient data (DAIMedLab, "Federico II" University of Naples; N° 252/18, October 2018). DNA samples were obtained from the patients after they had signed their informed consent, and according to the Declaration of Helsinki.

This research was funded by EHA Junior Research grant 3978026 (I.A.), and by Bando Star Linea 1 - Junior Principal Investigator grants COINOR, Università degli Studi di Napoli "Federico II" (R.R.) and Italian Minister of University and research (MIUR) PRIN project 2020 (A.I.).

Authorship

Contribution: I.A., R.R., and M.M. designed and conducted the study and prepared the manuscript; V.M. and F.C. performed differential proteomics and related statistical analyses; V.M. prepared the initial draft of the manuscript; B.E.R. and R.M. performed validation analyses by western blotting, vesiculation assay, and immunofluorescence; A.I. cared for the patients and provided a critical review of the manuscript; G.L.F., V.M.P., and S.U. cared for the patients; and V.C. performed the fluorescence-activated cell sorting analysis.

Conflict-of-interest disclosure: The authors declare no competing financial interests.

ORCID profiles: I.A., 0000-0003-0493-812X; V.M., 0000-0002-7459-8733; B.E.R., 0000-0001-5976-701X; R.M., 0000-0002-3084-0313; V.M.P., 0000-0002-8375-6289; G.L.F., 0000-0001-9833-1016; A.I., 0000-0002-9558-0356; R.R., 0000-0002-3624-7721.

Correspondence: Immacolata Andolfo, Department of Molecular Medicine and Medical Biotechnologies - "Federico II" University of Naples, Naples, Italy, CEINGE, Biotecnologie Avanzate, Franco Salvatore, Naples, Italy; email: immacolata.andolfo@unina.it; and Maria Monti, Department of Chemical Sciences - "Federico II" University of Naples, Naples, Italy, CEINGE, Biotecnologie Avanzate, Franco Salvatore, Naples, Italy; email: montimar@unina.it.

References

1. Cahalan SM, Lukacs V, Ranade SS, Chien S, Bandell M, Patapoutian A. Piezo1 links mechanical forces to red blood cell volume. *Elife*. 2015;4:e07370.
2. Jiang F, Yin K, Wu K, et al. The mechanosensitive Piezo1 channel mediates heart mechano-chemo transduction. *Nat Commun*. 2021;12(1):869.
3. Li J, Hou B, Tumova S, et al. Piezo1 integration of vascular architecture with physiological force. *Nature*. 2014;515(7526):279-282.
4. Ranade SS, Qiu Z, Woo SH, et al. Piezo1, a mechanically activated ion channel, is required for vascular development in mice. *Proc Natl Acad Sci U S A*. 2014;111(28):10347-10352.
5. Rode B, Shi J, Endesh N, et al. Piezo1 channels sense whole body physical activity to reset cardiovascular homeostasis and enhance performance. *Nat Commun*. 2017;8(1):350.
6. Solis AG, Bielecki P, Steach HR, et al. Mechanosensation of cyclical force by PIEZO1 is essential for innate immunity. *Nature*. 2019;573(7772):69-74.
7. Sun W, Chi S, Li Y, Ling S, et al. The mechanosensitive Piezo1 channel is required for bone formation. *Elife*. 2019;8:e47454.
8. Wang S, Chennupati R, Kaur H, et al. Endothelial cation channel PIEZO1 controls blood pressure by mediating flow-induced ATP release. *J Clin Invest*. 2016;126(12):4527-4536.
9. Albuisson J, Murthy SE, Bandell M, et al. Dehydrated hereditary stomatocytosis linked to gain-of-function mutations in mechanically activated PIEZO1 ion channels. *Nat Commun*. 2013;4:1884.
10. Andolfo I, Alper SL, De Franceschi L, et al. Multiple clinical forms of dehydrated hereditary stomatocytosis arise from mutations in PIEZO1. *Blood*. 2013;121(19):3925-3935.
11. Glogowska E, Schneider ER, Maksimova Y, et al. Novel mechanisms of PIEZO1 dysfunction in hereditary xerocytosis. *Blood*. 2017;130(16):1845-1856.
12. Picard V, Guitton C, Thuret I, et al. Clinical and biological features in PIEZO1-hereditary xerocytosis and Gardos channelopathy: a retrospective series of 126 patients. *Haematologica*. 2019;104(8):1554-1564.
13. Zarychanski R, Schulz VP, Houston BL, et al. Mutations in the mechanotransduction protein PIEZO1 are associated with hereditary xerocytosis. *Blood*. 2012;120(9):1908-1915.
14. Andolfo I, Russo R, Rosato BE, et al. Genotype-phenotype correlation and risk stratification in a cohort of 123 hereditary stomatocytosis patients. *Am J Hematol*. 2018;93(12):1509-1517.
15. Andolfo I, Russo R, Gambale A, Iolascon A. New insights on hereditary erythrocyte membrane defects. *Haematologica*. 2016;101(11):1284-1294.
16. Andolfo I, Russo R, Gambale A, Iolascon A. Hereditary stomatocytosis: An underdiagnosed condition. *Am J Hematol*. 2018;93(1):107-121.
17. Caulier A, Garcon L. PIEZO1, sensing the touch during erythropoiesis. *Curr Opin Hematol*. 2022;29(3):112-118.
18. Iolascon A, Andolfo I, Russo R. Advances in understanding the pathogenesis of red cell membrane disorders. *Br J Haematol*. 2019;187(1):13-24.
19. Tang H, Zeng R, He E, Zhang I, Ding C, Zhang A. Piezo-type mechanosensitive ion channel component 1 (Piezo1): a promising therapeutic target and its modulators. *J Med Chem*. 2022;65(9):6441-6453.
20. Coste B, Xiao B, Santos JS, et al. Piezo proteins are pore-forming subunits of mechanically activated channels. *Nature*. 2012;483(7388):176-181.
21. Ge J, Li W, Zhao Q, et al. Architecture of the mammalian mechanosensitive Piezo1 channel. *Nature*. 2015;527(7576):64-69.
22. Guo YR, MacKinnon R. Structure-based membrane dome mechanism for Piezo mechanosensitivity. *Elife*. 2017;6:e33660.
23. Jiang Y, Yang X, Jiang J, Xiao B. Structural designs and mechanogating mechanisms of the mechanosensitive Piezo channels. *Trends Biochem Sci*. 2021;46(6):472-488.
24. Saotome K, Murthy SE, Kefauver JM, Whitwam T, Patapoutian A, Ward AB. Structure of the mechanically activated ion channel Piezo1. *Nature*. 2018;554(7693):481-486.
25. Zhao Q, Zhou H, Chi S, et al. Structure and mechanogating mechanism of the Piezo1 channel. *Nature*. 2018;554(7693):487-492.
26. Ma S, Cahalan S, LaMonte G, et al. Common PIEZO1 allele in African populations causes RBC dehydration and attenuates plasmodium infection. *Cell*. 2018;173(2):443-455.e12.
27. Ilboudo Y, Bartolucci P, Garrett ME, et al. A common functional PIEZO1 deletion allele associates with red blood cell density in sickle cell disease patients. *Am J Hematol*. 2018;93(11):E362-E365.
28. Nguetse CN, Purington N, Ebel ER, et al. A common polymorphism in the mechanosensitive ion channel PIEZO1 is associated with protection from severe malaria in humans. *Proc Natl Acad Sci U S A*. 2020;117(16):9074-9081.
29. Andolfo I, Rosato BE, Manna F, et al. Gain-of-function mutations in PIEZO1 directly impair hepatic iron metabolism via the inhibition of the BMP/SMADs pathway. *Am J Hematol*. 2020;95(2):188-197.
30. Ma S, Dubin AE, Zhang Y, et al. A role of PIEZO1 in iron metabolism in mice and humans. *Cell*. 2021;184(4):969-982.e13.
31. Caulier A, Jankovsky N, Demont Y, et al. PIEZO1 activation delays erythroid differentiation of normal and hereditary xerocytosis-derived human progenitor cells. *Haematologica*. 2020;105(3):610-622.
32. Palinski W, Monti M, Camerlingo R, et al. Lysosome purinergic receptor P2X4 regulates neoangiogenesis induced by microvesicles from sarcoma patients. *Cell Death Dis*. 2021;12(9):797.

33. Salzer U, Zhu R, Luten M, et al. Vesicles generated during storage of red cells are rich in the lipid raft marker stomatin. *Transfusion*. 2008;48(3):451-462.
34. Gamonet C, Desmarets M, Mourey G, et al. Processing methods and storage duration impact extracellular vesicle counts in red blood cell units. *Blood Adv*. 2020;4(21):5527-5539.
35. Andolfo I, Martone S, Rosato BE, et al. Complex Modes of Inheritance in Hereditary Red Blood Cell Disorders: A Case Series Study of 155 Patients. *Genes (Basel)*. 2021;12(7):958.
36. Knight T, Zaidi AU, Wu S, Gadgeel M, Buck S, Ravindranath Y. Mild erythrocytosis as a presenting manifestation of PIEZO1 associated erythrocyte volume disorders. *Pediatr Hematol Oncol*. 2019;36(5):317-326.
37. Russo R, Andolfo I, Manna F, et al. Multi-gene panel testing improves diagnosis and management of patients with hereditary anemias. *Am J Hematol*. 2018;93(5):672-682.
38. Zama D, Giulietti G, Muratore E, et al. A novel PIEZO1 mutation in a patient with dehydrated hereditary stomatocytosis: a case report and a brief review of literature. *Ital J Pediatr*. 2020;46(1):102.
39. Greenwalt TJ. The how and why of exocytic vesicles. *Transfusion*. 2006;46(1):143-152.
40. Prado GN, Romero JR, Rivera A. Endothelin-1 receptor antagonists regulate cell surface-associated protein disulfide isomerase in sickle cell disease. *FASEB J*. 2013;27(11):4619-4629.
41. Yang Y, Neo SY, Chen Z, et al. Thioredoxin activity confers resistance against oxidative stress in tumor-infiltrating NK cells. *J Clin Invest*. 2020;130(10):5508-5522.
42. Cao M, Yuan W, Peng M, et al. Role of CyPA in cardiac hypertrophy and remodeling. *Biosci Rep*. 2019;39(12):BSR20193190.
43. Zheng S, Krump NA, McKenna MM, et al. Regulation of erythrocyte Na(+)/K(+)/2Cl(-) cotransport by an oxygen-switched kinase cascade. *J Biol Chem*. 2019;294(7):2519-2528.
44. Vitari AC, Deak M, Morrice NA, et al. The WNK1 and WNK4 protein kinases that are mutated in Gordon's hypertension syndrome phosphorylate and activate SPAK and OSR1 protein kinases. *Biochem J*. 2005;391(Pt 1):17-24.
45. Coste B, Mathur J, Schmidt M, et al. Piezo1 and Piezo2 are essential components of distinct mechanically activated cation channels. *Science*. 2010;330(6000):55-60.
46. Zhou Z. Structural Analysis of Piezo1 Ion Channel Reveals the Relationship between Amino Acid Sequence Mutations and Human Diseases. *Journal of Biosciences and Medicines*. 2019;7(12):139-155.
47. Zhang DL, Wu J, Shah BN, et al. Erythrocytic ferroportin reduces intracellular iron accumulation, hemolysis, and malaria risk. *Science*. 2018;359(6383):1520-1523.
48. Deshpande CN, Ruwe TA, Shawki A, et al. Calcium is an essential cofactor for metal efflux by the ferroportin transporter family. *Nat Commun*. 2018;9(1):3075.
49. Yang X, Lin C, Chen X, Li S, Li X, Xiao B. Structure deformation and curvature sensing of PIEZO1 in lipid membranes. *Nature*. 2022;604(7905):377-383.
50. Buyan A, Cox CD, Barnoud J, et al. Piezo1 Forms Specific, Functionally Important Interactions with Phosphoinositides and Cholesterol. *Biophys J*. 2020;119(8):1683-1697.
51. Jin Y, Liang Q, Tieleman DP. Interactions between band 3 anion exchanger and lipid nanodomains in ternary lipid bilayers: atomistic simulations. *J Phys Chem B*. 2020;124(15):3054-3064.
52. Thangaraju K, Neerukonda SN, Katneni U, Buehler PW. Extracellular vesicles from red blood cells and their evolving roles in health, coagulopathy and therapy. *Int J Mol Sci*. 2020;22(1):153.
53. Daou Y, Falabrègue M, Pourzand C, Peyssonnaux C, Edeas M. Host and microbiota derived extracellular vesicles: Crucial players in iron homeostasis. *Front Med (Lausanne)*. 2022;9:985141.
54. Tzounakas VL, Dzieciatkowska M, Anastasiadi AT, et al. Red cell proteasome modulation by storage, redox metabolism and transfusion. *Blood Transfus*. 2022;20(1):27-39.